Supplementary Information (SI) for Nanoscale Horizons.

Supporting Information:

SI Fig. A: Optical photograph of a typical papaya plant found in India.

Characterizations

The structural analysis of powder sample derived from papaya seeds PC, HLC, and HFC was first carried out using an X-ray diffractometer (XRD, D8 advance, Bruker AXS) using Cu Kα-radiations (λ = 1.5418 Å). The surface morphological and compositional studies were executed using a scanning electron microscope (SEM, JEOLJSM 6360 A, Japan) and a Field Emission Scanning Electron Microscope (FESEM, Carl Zeiss, Merlin 6073). Furthermore, structural characterization was performed by a Raman spectrometer with a laser

excitation wavelength of 532 nm using the Renishaw inVia instrument. Moreover, in-depth structural and morphological investigations were performed using transmission electron microscopy (TEM, Technai G2 20 Twin, FEI) operated in high resolution (HR) and electron diffraction (ED) modes. The chemical analysis of seeds was carried out using X-ray photoelectron spectroscopy (XPS, VG Microtech ESCA 3000). The work function was measured using a UPS analysis system consisting of a hemispherical energy analyzer (VG Microtech ESCA 3000) and a UV (He I, 21.2 eV) source. The Brunauer–Emmet–Teller (BET) surface area of the prepared samples was calculated from the N_2 adsorption isotherms at liquid N_2 temperature using the Quantachrome NOVATouch LX1 instrument. The sample was degassed in a vacuum at 100 °C for 2 h before the BET analysis.

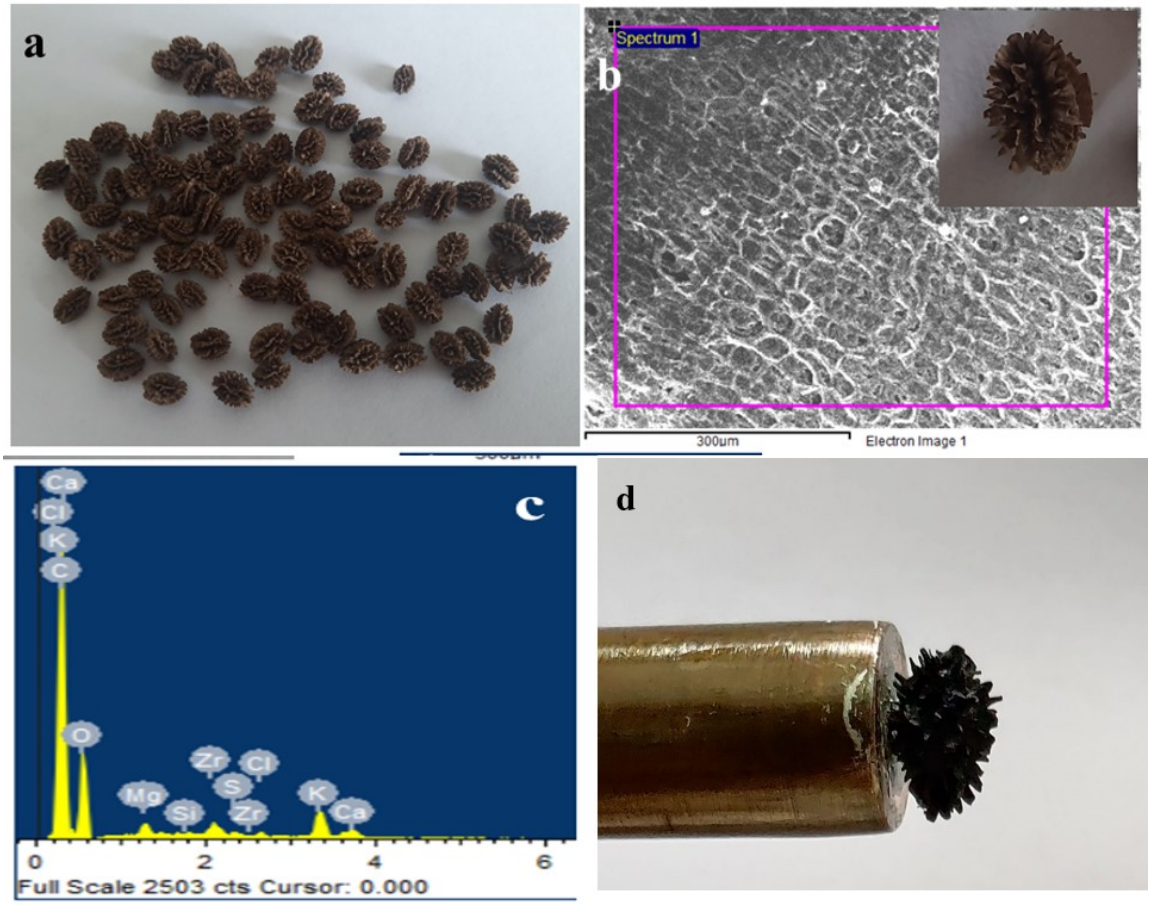

SI Fig. 1. (a) Photograph, (b) SEM image (c) EDS pattern of bare papaya seeds sample and d) photograph of seed attached metal rod.

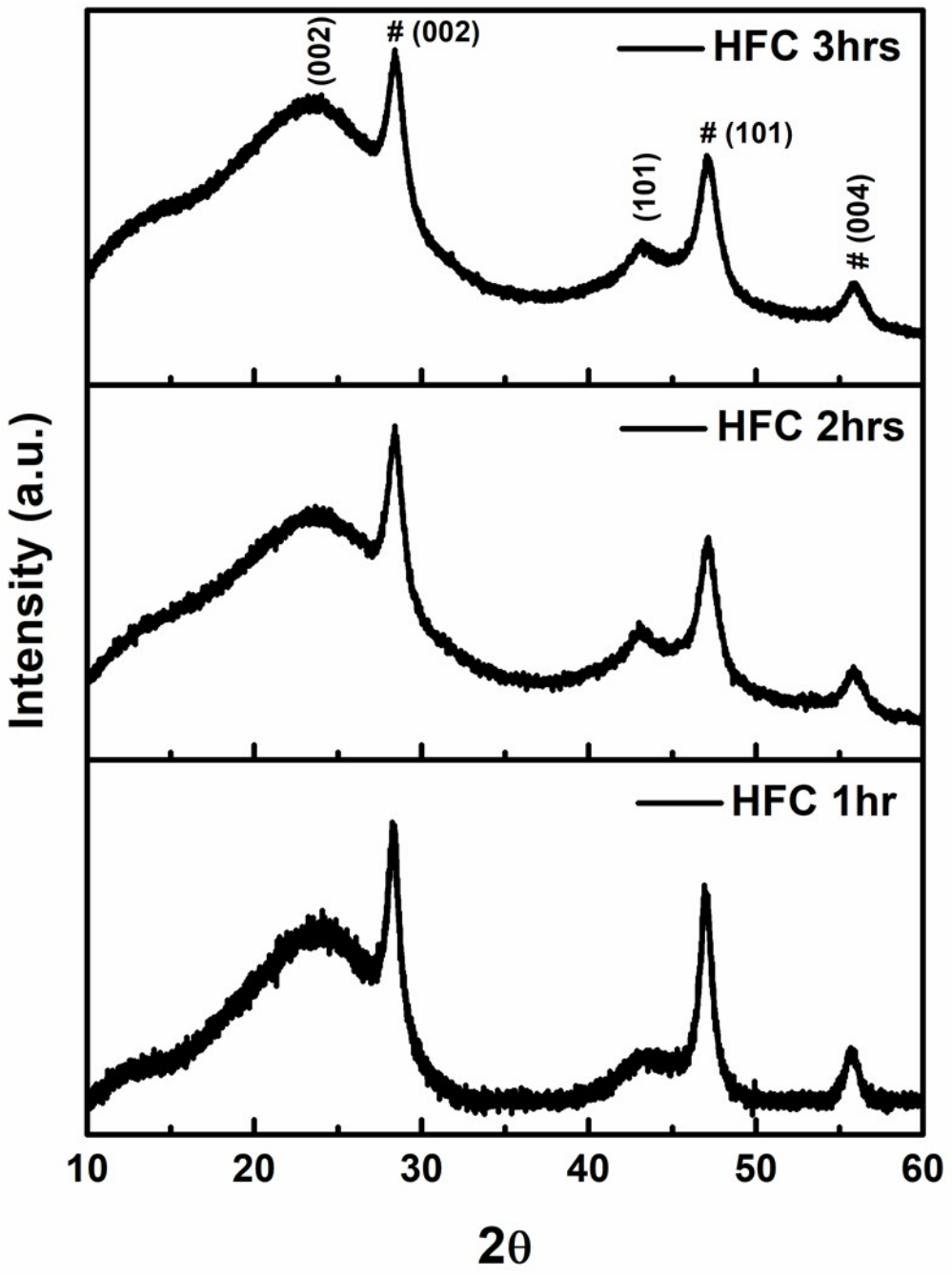

SI Fig. 2. XRD pattern of HFC powder samples synthesized at 800 °C for 1, 2 and 3 h.

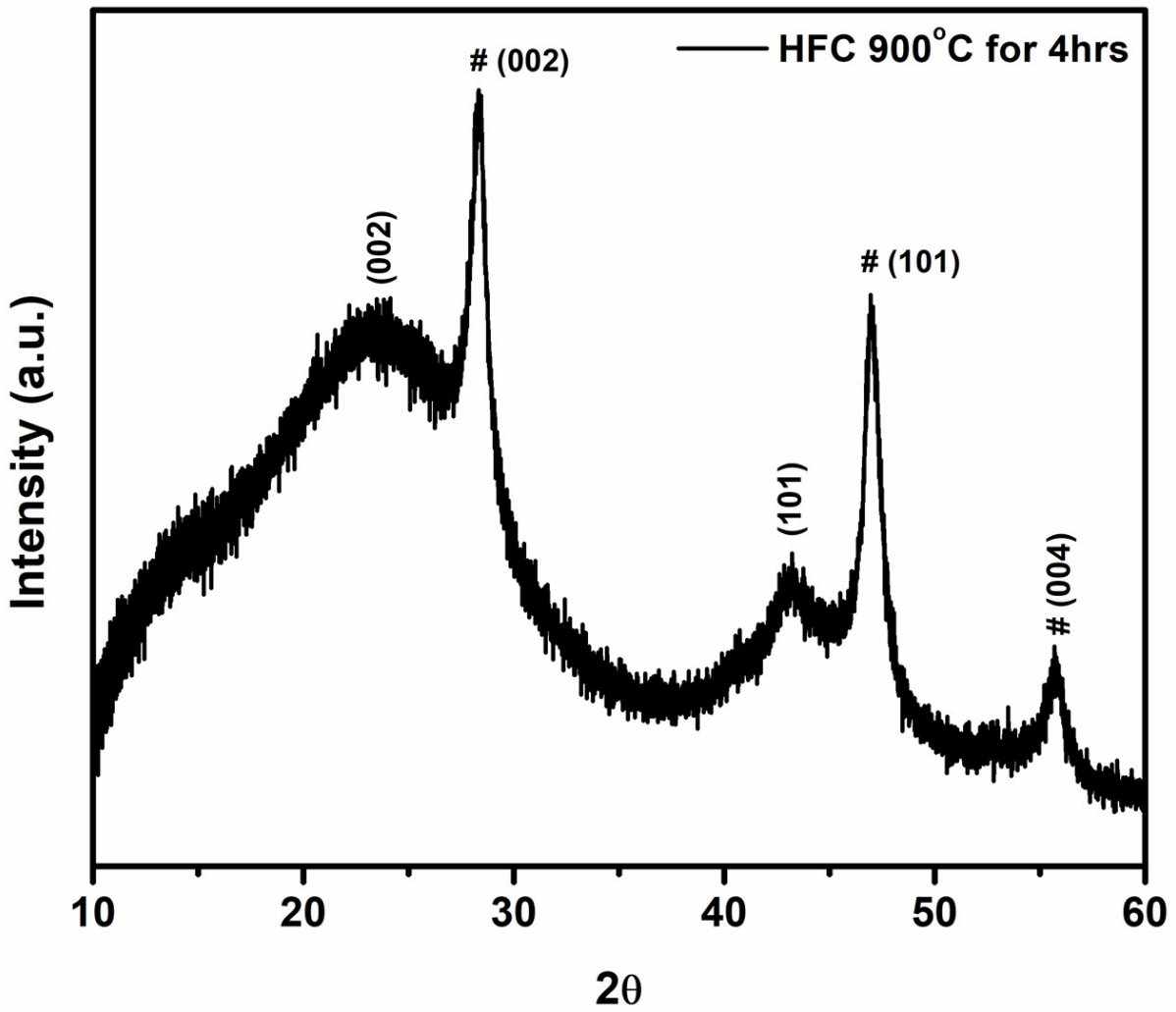

SI Fig. 3. XRD pattern of HFC powder samples synthesized at 900°C for 4 h

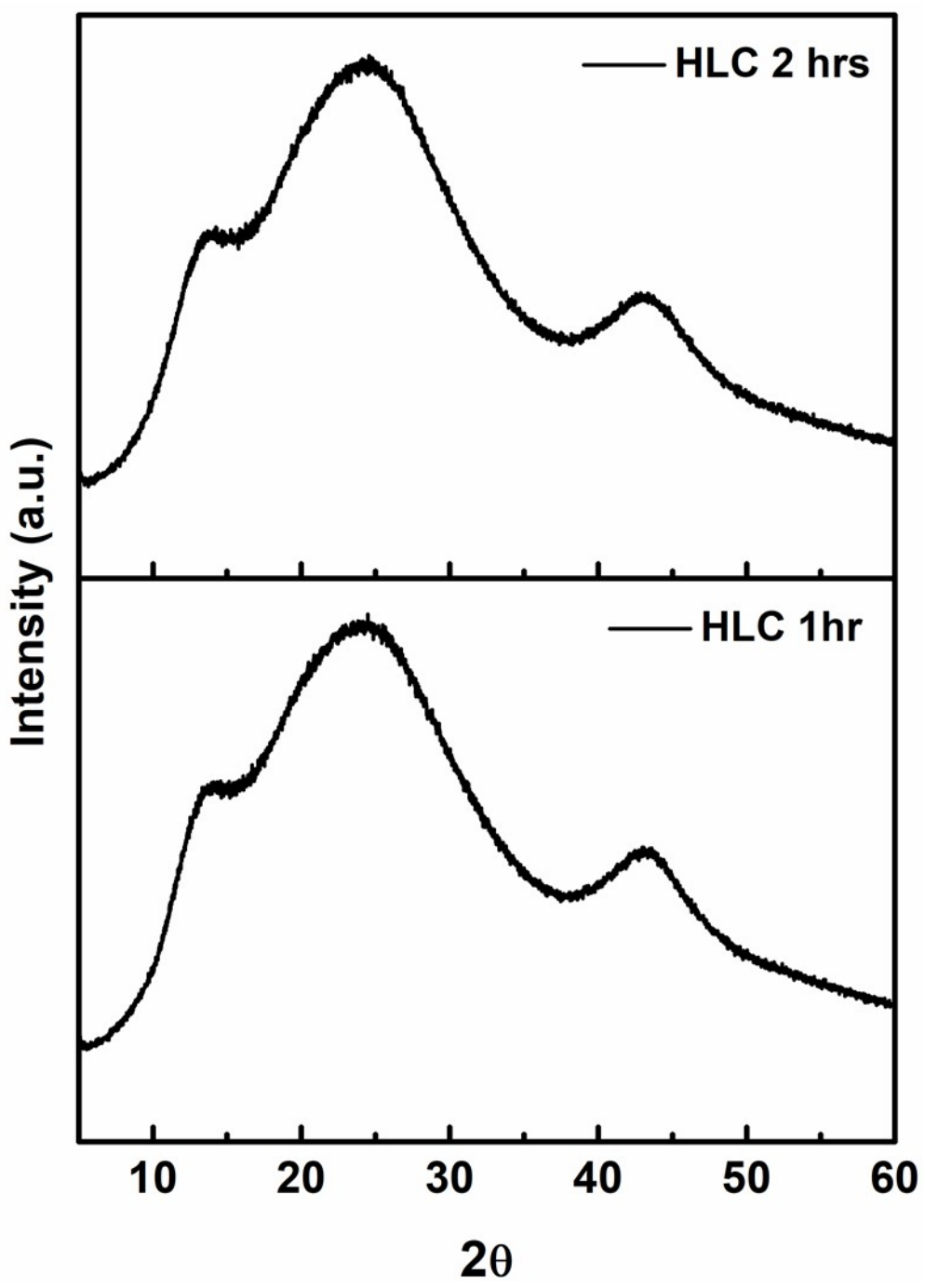

SI Fig.4. XRD pattern of HLC powder samples synthesized at 800°C for 1 and 2 h.

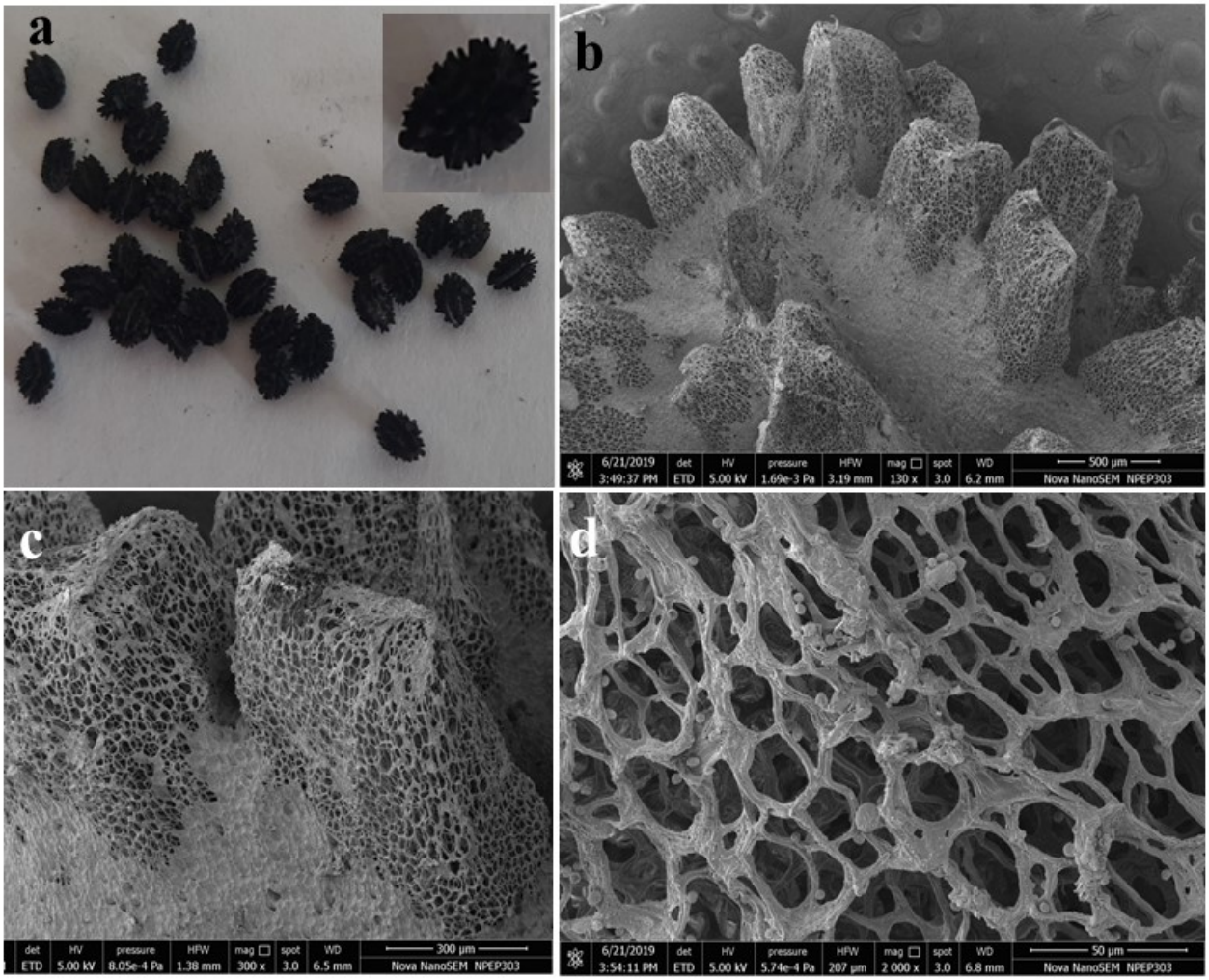

SI Fig. 5. (a) Photograph of PC seeds sample (at 800°C for 1h) with corresponding SEM image shown in (b-d).

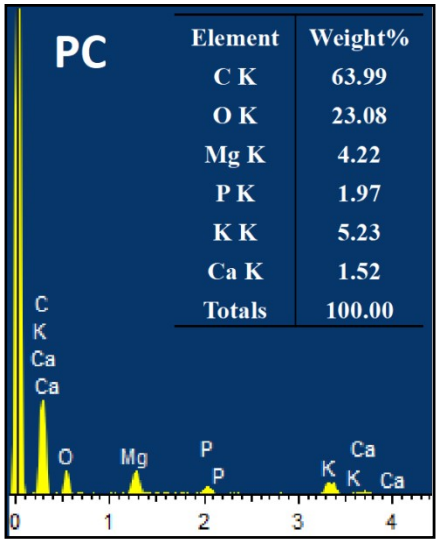

SI Fig. 6. EDS spectra of PC sample (at 800°C for 1hr) with an inset show the elemental analysis.

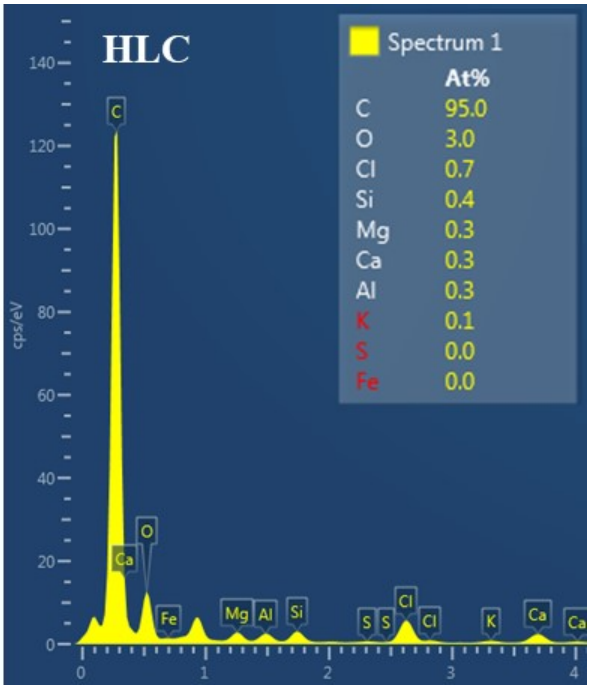

SI Fig. 7. EDS spectra of HLC sample (at 800°C for 1hr) with an inset show the elemental analysis.

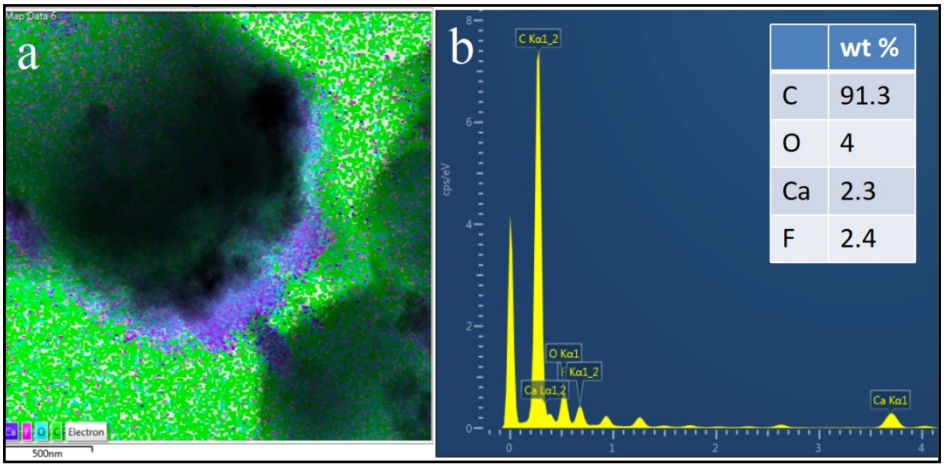

SI Fig. 8. (a)Mapping image and b) EDS spectra of HFC sample (at 800°C for 1hr) with an inset show the elemental analysis.

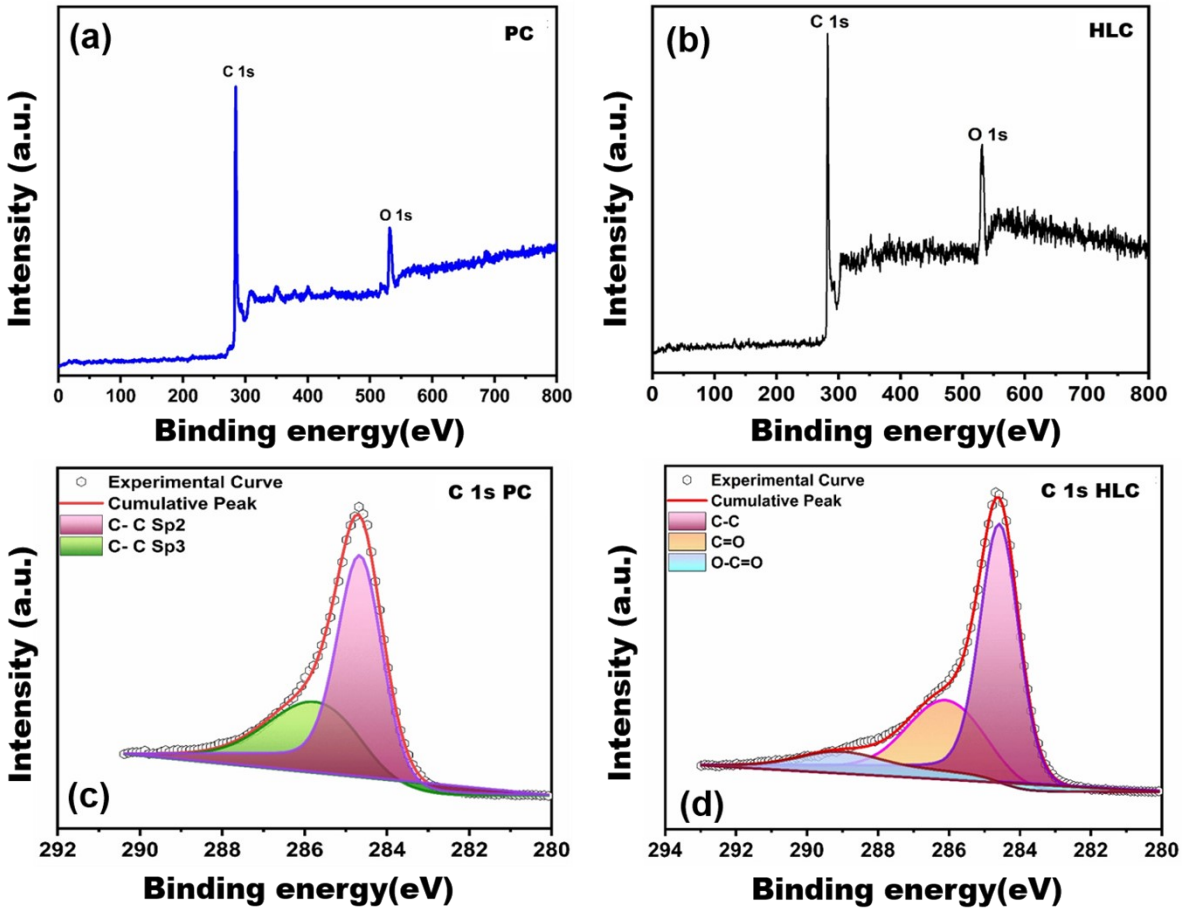

SI Fig. 9 a-b) XPS survey spectra, (c-d) high-resolution XPS C 1s spectra of PC and HLC samples.

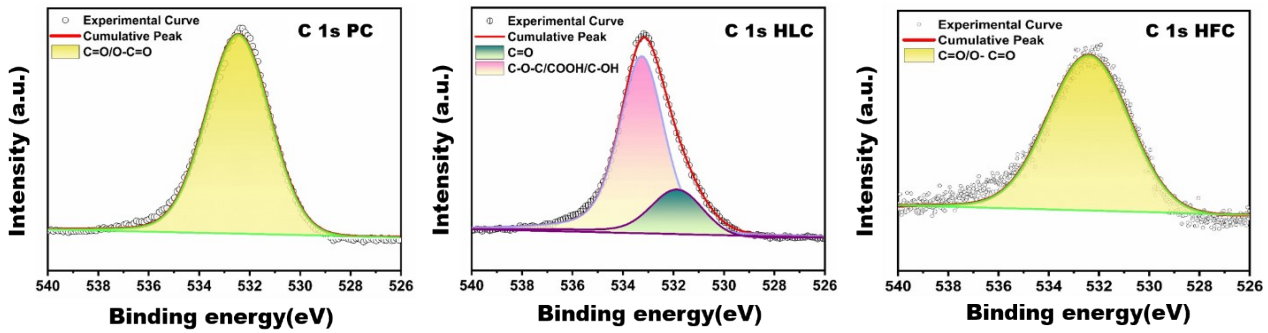

SI Fig. 10 High-resolution XPS O 1s spectra of PC, HLC and HFC samples.

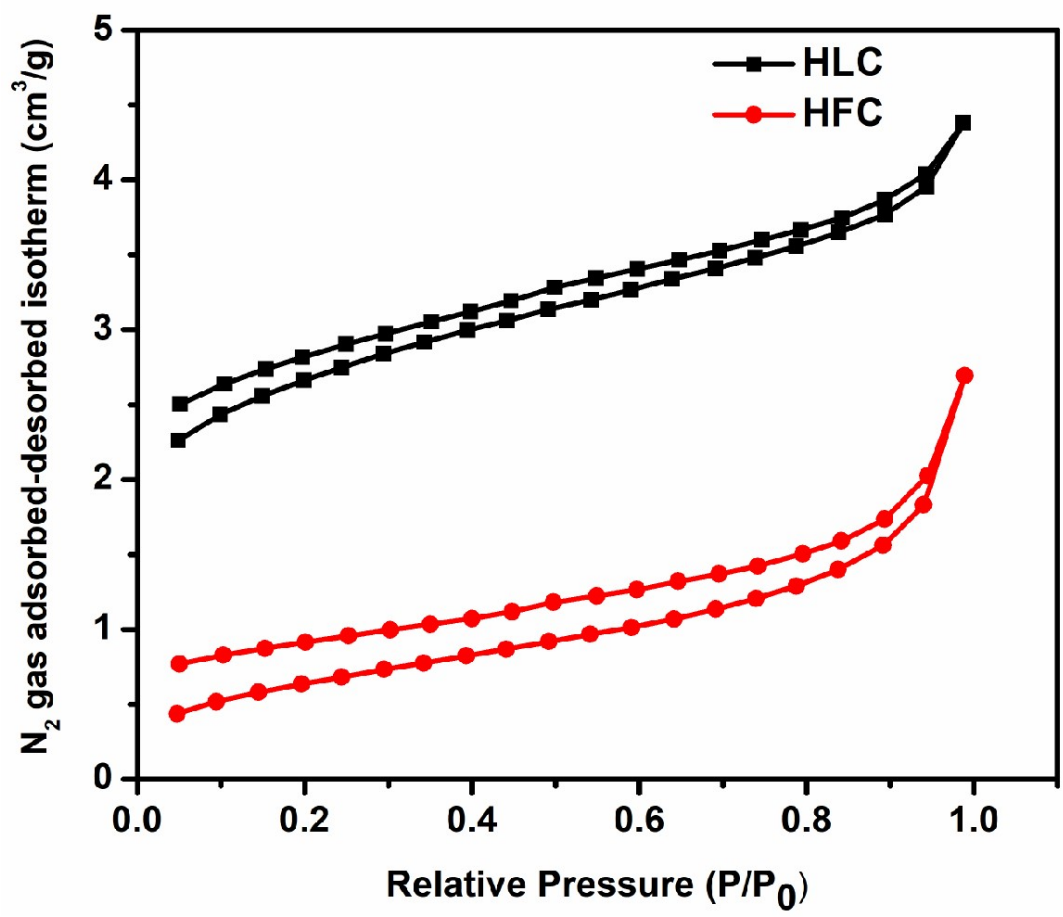

SI Fig. 11 BET N_2 gas adsorbed–desorbed isotherm curve of HLC and HFC samples. The pore size of the HLC and HFC samples (SI Fig. 12) showed different levels of pores. The HLC and HFC samples had a pore diameter less than 15 nm with a maximum diameter of ~7 nm indicating that are mesoporous in nature.

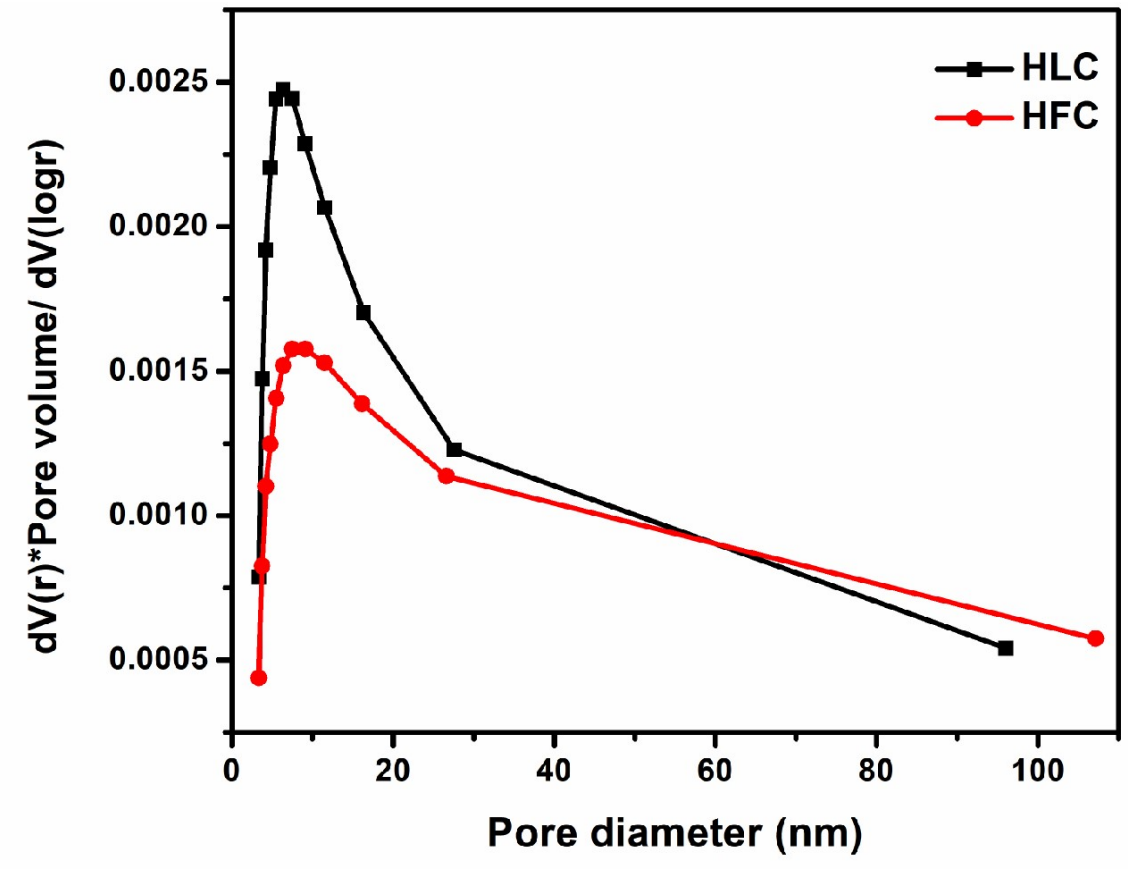

SI Fig. 12 BJH pore size distribution curves of HLC and HFC samples.

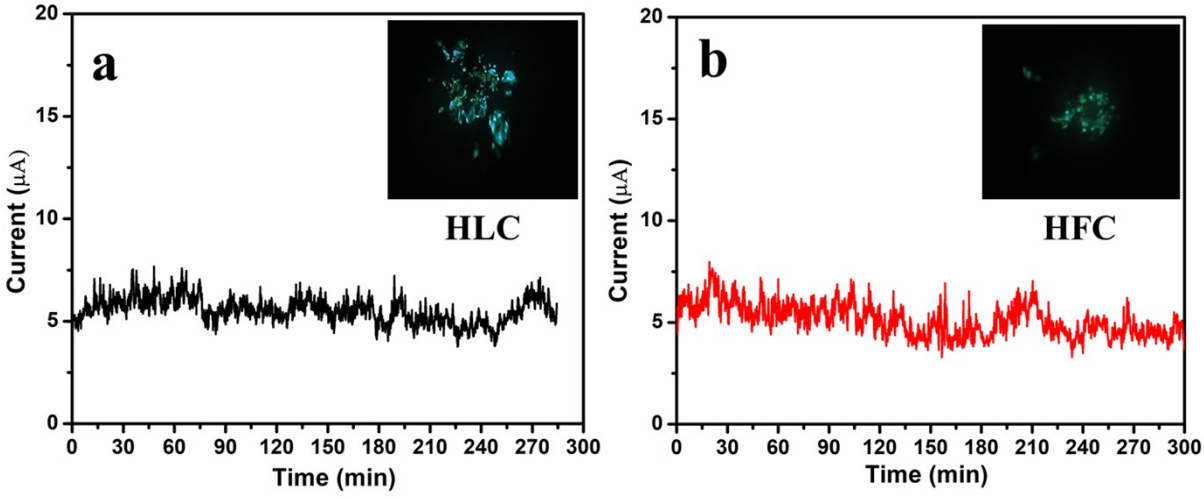

SI Fig. 13 Field emission current stability (I–t) plot of (a) HLC and (b) HFC seed emitters recorded at the base pressure of 1×10^{-8} mbar at pre-set value ~5 μA with the FE image shown in the inset.

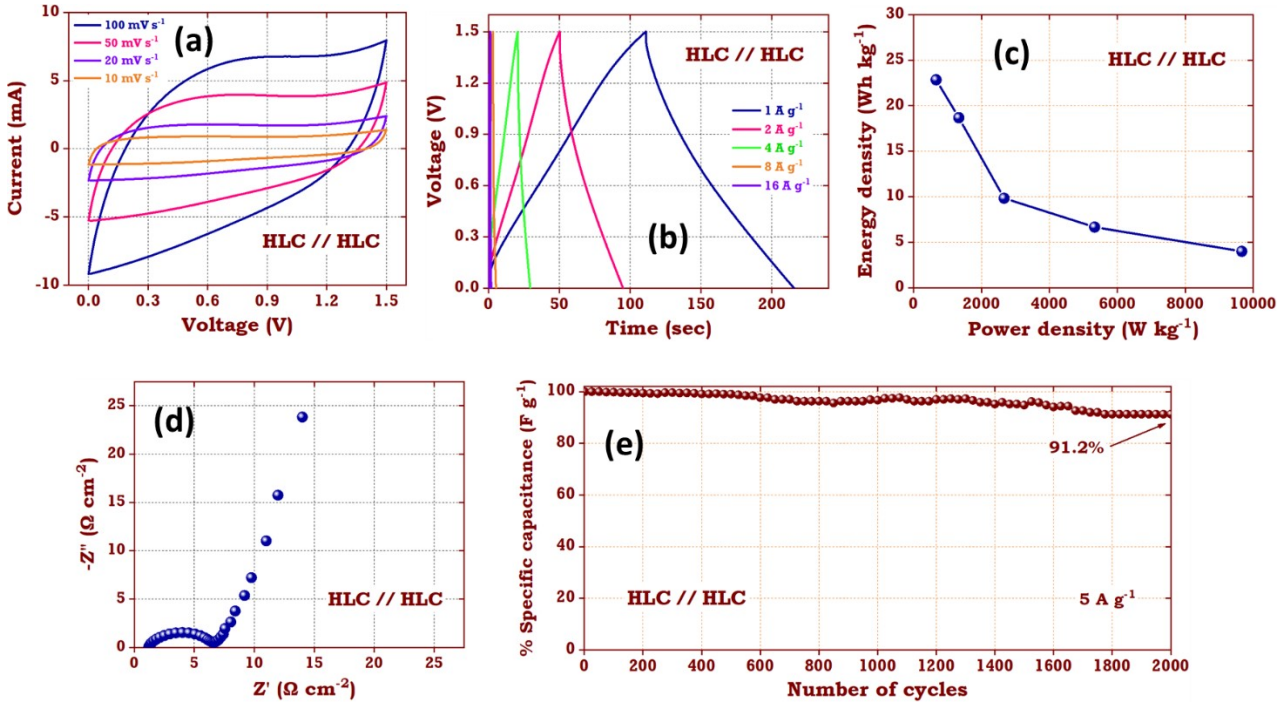

SI Fig. 14 (a) CV, (b) GCD, (c) Ragone plot, (d) Nyquist plot and (e) Cyclic stability of HLC // HLC coin cell supercapacitor device.

The figure 14 depicts the electrochemical measurements of HLC // HLC symmetric coin cell supercapacitor device. In CV measurement (Figure 14a), the HLC // HLC device shows the nearly rectangular shape within voltage window of 1.5 V with no sharp increase or decrease in the current due to electrolysis of water. This reactangular shape without any redox peaks implies the EDLC behaviour of the HLC sample. Figure 14 b shows the GCD curves of the HLC // HLC supercapacitor device performed at current density of 1 to 16 A g^{-1}. The symmetric charging discharging curves indicated the ideal supercapacitor behaviour of the fabricated device. This device posseses the highest specific capacitance of 73 F g^{-1} at 1 A g^{-1}. From the GCD curves, the energy and power density values were calculated using equation 5 and 6. The relationship between the energy and power density is shown in figure 14 c. The fabricated device demonstrated maximum energy density value of 22.8 Wh kg^{-1} at 1 A g^{-1} and maximum power density of 9666 W kg^{-1} at 16 A g^{-1}. Additionally, the EIS measurements were carried out over the fabricated HLC // HLC supercapacitor device, which shows low internal resistance

value with surface faradic reaction kinetics. Along with the straight line slope in the lower frequency region (Warburg resistance) indicating the capacitive nature of the HLC // HLC symmetric supercapacitor device. The cyclic stability of the HLC // HLC supercapacitor device was also tested for 2000 cycles at 5 A g^{-1}. This device displays the 91.2% of its initial specific capacitance after 2000 charging-discharging cycles.